Bioorganic Chemistry 117 (2021) 105411

Contents lists available at ScienceDirect

Bioorganic Chemistry

journal homepage: www.elsevier.com/locate/bioorg

Guided rational design with scaffold hopping leading to novel histamine H_3 receptor ligands

Nakisa Ghamari [a,b], Saeed Kouhi Hargelan [b], Aleksandra Zivkovic [c], Luisa Leitzbach [c], Siavoush Dastmalchi [a,b], Holger Stark [c,*], Maryam Hamzeh-Mivehroud [a,b,*]

[a] Biotechnology Research Center, Tabriz University of Medical Sciences, Tabriz, Iran
[b] School of Pharmacy, Tabriz University of Medical Sciences, Tabriz, Iran
[c] Heinrich Heine University Düsseldorf, Institute of Pharmaceutical and Medicinal Chemistry, Universitaetsstr. 1, D-40225 Duesseldorf, Germany

ARTICLE INFO

Keywords:
Histamine H_3 receptor
Scaffold hopping
Molecular docking
Molecular dynamics simulation
H_3R antagonist
Synthesis

ABSTRACT

During the past decades, histamine H_3 receptors have received widespread attention in pharmaceutical research due to their involvement in pathophysiology of several diseases such as neurodegenerative disorders. In this context, blocking of these receptors is of paramount importance in progression of such diseases. In the current investigation, novel histamine H_3 receptor ligands were designed by exploiting scaffold-hopping drug-design strategy. We inspected the designed molecules in terms of ADME properties, drug-likeness, as well as toxicity profiles. Additionally molecular docking and dynamics simulation studies were performed to predict binding mode and binding free energy calculations, respectively. Among the designed structures, we selected compound **d2** and its demethylated derivative as examples for synthesis and affinity measurement. *In vitro* binding assays of the synthesized molecules demonstrated that **d2** has lower binding affinity (K_i = 2.61 μM) in radioligand displacement assay to hH_3R than that of demethylated form (K_i = 12.53 μM). The newly designed compounds avoid of any toxicity predictors resulted from extended in silico and experimental studies, can offer another scaffold for histamine H_3R antagonists for further structure–activity relationship studies.

1. Introduction

Histamine as biogenic multifunctional amine is involved in wide variety of physiological processes via four distinct subtypes of G-protein coupled histamine receptors (H_1, H_2, H_3, and H_4). Since the identification of H_3 receptors over the nearly four decades, versatile potential of this receptor in physiological processes have been elucidated [1]. This receptor is located pre-synaptically as auto- and heteroreceptor in central nervous system (CNS) responsible for modulating the release of histamine and other neurotransmitters such as acetylcholine, γ-aminobutyric acid (GABA), dopamine, serotonin, and noradrenaline via a negative feedback mechanism [2]. For the past decades of research, the importance of H_3R in neurological disorders has been well explored and hence it can be considered as a therapeutic potential target in such diseases. Attention deficit hyperactivity disorder (ADHD), Alzheimer's disease, schizophrenia, learning and memory disorders, Parkinson's disease and sleep disorders, and epilepsy are examples of neuronal abnormalities and impairments that can be treated by H_3R antagonists and inverse agonists [3]. Based on ever growing number of H_3R related candidate molecules in different phases of clinical trials [4], it is anticipated that these types of agents might become drugs of future in neurodegenerative diseases beneficial especially for elderly population.

Launching a therapeutic agent from idea to market necessitates considerable amounts of time and cost in a process known as drug design and discovery. Shortening this process is a high priority for scientists working in this field. Undoubtedly, integration of computational approaches and experimental methods synergistically fulfill this task in a timely and cost effective manner. The main objectives followed in computer-aided drug design (CADD) are: *i)* filtering the large libraries against target of interest in a procedure called "virtual screening" to reach the bioactive lead compounds, *ii)* lead optimization step in order to achieve favorable compounds in terms of developmental potential [5].

The key elements in the context of lead optimization are scaffold hopping and bioisosteric replacement aiming to improve potency, drug-like properties and safety profiles of the lead compounds. Scaffold

* Corresponding authors at: Biotechnology Research Center, Tabriz University of Medical Sciences, Tabriz, Iran (M. Hamzeh-Mivehroud) and Heinrich Heine University Düsseldorf, Institute of Pharmaceutical and Medicinal Chemistry, Duesseldorf, Germany (H. Stark).
E-mail addresses: stark@hhu.de (H. Stark), hamzehm@tbzmed.ac.ir (M. Hamzeh-Mivehroud).

https://doi.org/10.1016/j.bioorg.2021.105411
Received 9 September 2021; Received in revised form 3 October 2021; Accepted 4 October 2021
Available online 8 October 2021

hopping (or lead hopping) is defined as structural decoration of a given molecule by replacing the available scaffolds for introducing new chemotypes with improved properties. Indeed, the main emphasis of scaffold hopping has been put on altering the properties of the molecule by moving it into novel chemical space while retaining the biological activity. This approach is routinely employed for a number of reasons such as prohibited structural motifs responsible for toxicity, unwanted side effects, metabolic liabilities, and undesirable physicochemical properties. Evidently, chemical synthesizability of the designed compounds should be taken into account in rational drug design. The most principal approaches in scaffold hopping are shape matching, pharmacophore searching, fragment replacement and similarity search [6–8].

The only marketed histamine H_3R antagonist/inverse agonist is pitolisant (Wakix®) approved by the European Medicines Agency available in the European Union for treatment of narcolepsy with or without cataplexy [9,10]. However, there is ongoing interest in identification of novel histamine H_3R antagonists/inverse agonists for treatment of neurological impairments and still some of them are in clinical trials for a range of indications [11–21]. Previously, we have identified two compounds capable of binding to H_3R in the submicromolar K_i range using radioligand displacement studies [22]. The introduced lead compounds were also functional in terms of antagonist activity [23]. The aim of the present study was structural optimization of these computationally identified lead compounds in order to improve physicochemical properties useful in neurological disorders.

2. Results

2.1. Scaffold-hopping analysis

In the current study, scaffold-hopping analysis was used on previously identified H_3R antagonists (Fig. 1) aiming to improve biological activity and eliminate potential toxicophores. The procedure was started with exhaustive fragmentation of these molecules along the single non-ring bonds followed by selection of each portion serving as a query for database search using bioisosteric replacement tool implemented in Spark program. To this end, the resulting fragments were subjected to iterative seeking procedure for finding similar bioisosters and fragments to that of original entity in terms of shape and electronic properties in the region of interest. Based on the calculated field point patterns, the fragments were derived from ChEMBL and Zinc database available in Spark program. Upon the generation of virtual library, a diverse array of ligands with novel chemotypes were sorted out based on a scaled score called bioisostere factor (BIF%). The greater positive value of BIF score is indicative of favorable bioisostere with higher similarity to the starter molecule from geometrical viewpoint. Likewise, the negative BIF value reflects that the fragment is not appropriate for the replaced moiety. Finally, top-scoring entities were carefully inspected according to the features associated with field and shape scores, radial plots, and unstable/reactive functionality.

2.2. ADME, Drug-Likeness and toxicity property analysis

The retrieved compounds from scaffold-hopping analysis were filtered on the basis of pharmacokinetic and drug-likeness parameters calculated by SwissADME online webserver. Fig. 2 and Supplementary Table S1 represent the structure of top-ranked candidates with desirable physicochemical parameters, pharmacokinetics, drug-likeness, and medicinal chemistry friendliness. The selected compounds were predicted to be of orally bioavailable inferred from their optimal physicochemical properties fall within desired range. Furthermore, it was predicted that the compounds were expected to have the ability for gastrointestinal absorption and blood–brain barrier (BBB) permeability. Moreover, all the selected candidates encompassed the different drug-likeness properties proposed by Lipinski [24], Ghose [25], Egan [26], Muegge [27], and Veber [28]. Additionally, the molecules were free from potentially problematic fragments reported in promiscuous compounds using pan-assay interference compounds (PAINS) [29] and Brenk [30] filters. The tendency of the selected compounds for being substrate of P-glycoprotein (P-gp) and cytochrome P450 enzymes were also investigated and shown in Supplementary Table S1. The other critical factor considered in the filtering process was synthetic

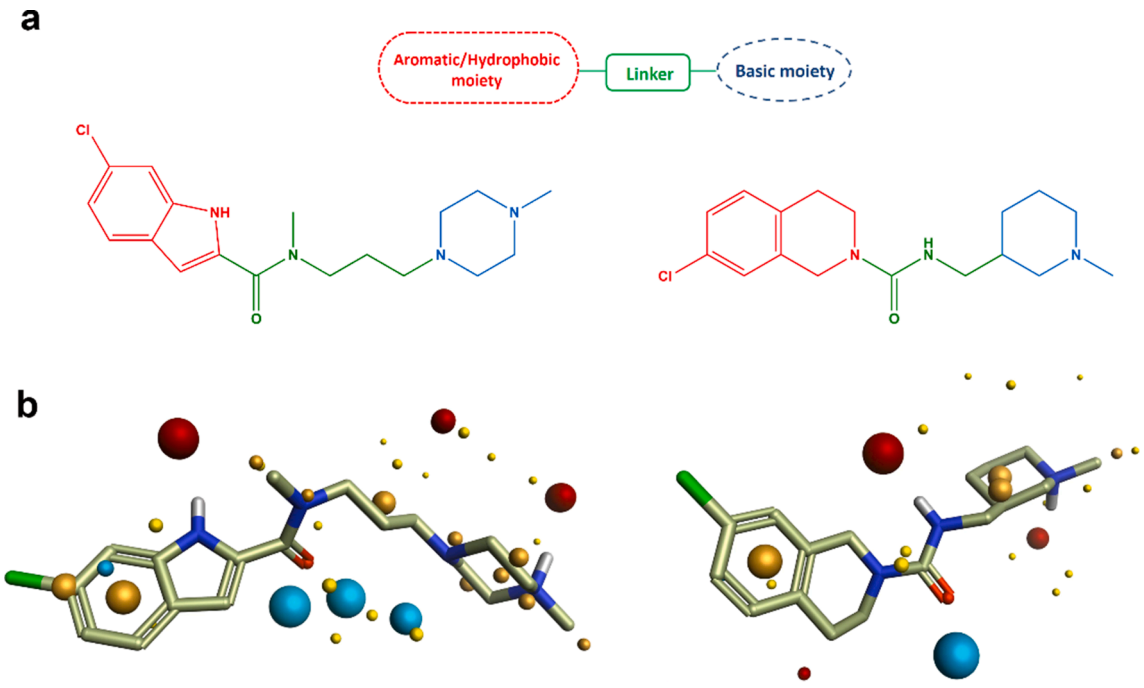

Fig. 1. **(a)** Schematic representation of the pharmacophore model proposed for H_3R antagonists along with structure of previously identified compounds as starter molecules for scaffold hopping analysis **(b)** Calculated field point patterns represented for the query molecules. Negatively charged field points are shown in blue; positively charged field points are red; van der Waals/shape field points are displayed in yellow; centers of hydrophobicity are shown in orange. (For interpretation of the references to colour in this figure legend, the reader is referred to the web version of this article.)

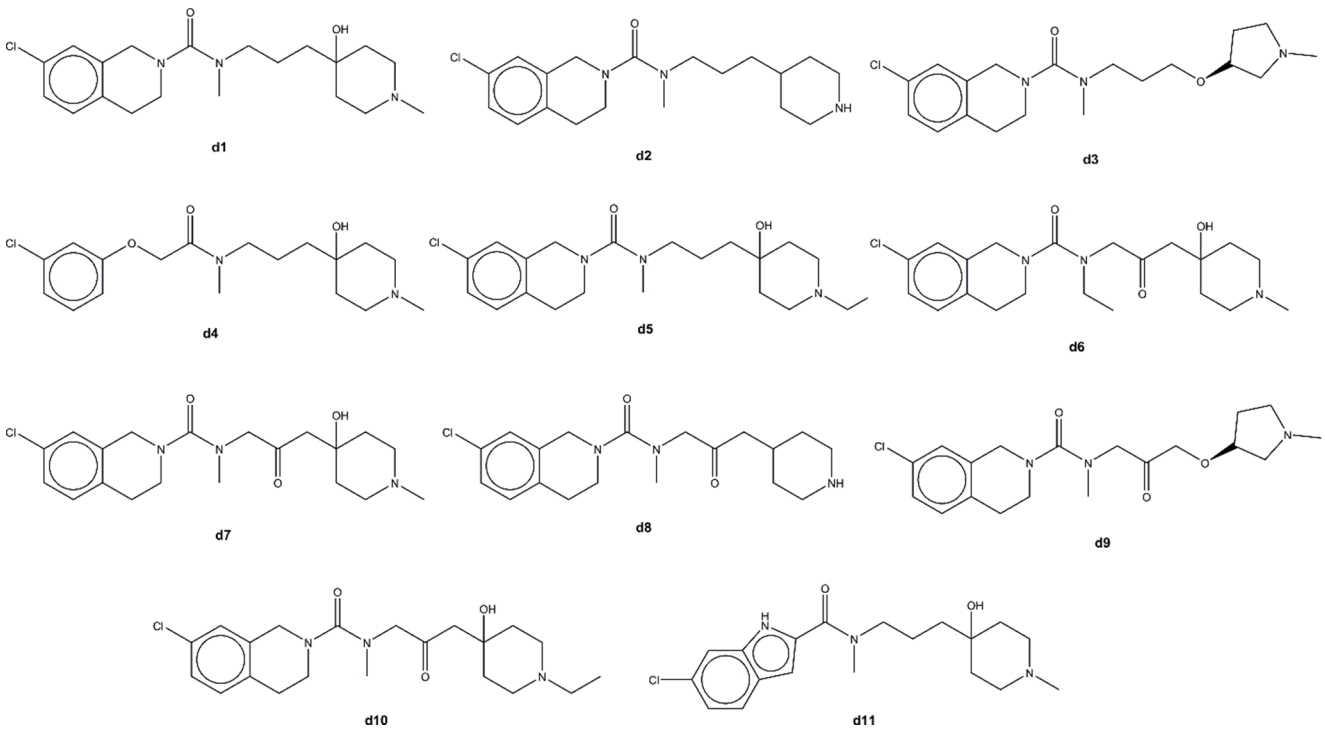

Fig. 2. Chemical structures of designed compounds as H_3R antagonists.

tractability of the designed molecules. The analysis demonstrated that the chemical synthesis of all the proposed molecules is feasible deduced from low synthetic accessibility score shown in Supplementary Table S1. The candidate molecules were also investigated according to their possible binding affinity towards H_3R using SwissTargetPrediction webserver and those compounds with highest probability of affinity to H_3R were progressed to the next steps of analyses. To gain insight into CNS drug likeness of the candidates, MPO analysis was performed across a range of physicochemical property space determining CNS permeability. The result of MPO analysis for the selected compounds presented in Supplementary Table S2 showed that all molecules passed the threshold of MPO score considered for marketed CNS drugs (MPO desirability score ≥ 4 in a scale of 0–6). For toxicological profile analysis of the selected compounds, OpenVirtualToxLab platform was used. Based on predicted TP values for the selected compounds shown in Supplementary Table S3, most of them are categorized in class 0 in the scale of toxicity alert suggesting the possible safety of the candidate molecules.

2.3. *Molecular docking and calculation of binding free energy for ligand-receptor complex*

Following applying different filtering criteria on the designed compounds, molecular docking calculations were used to determine the binding mode of the selected candidate molecules towards H_3R using GOLD program. Fig. 3 provides 2D and 3D illustrations for **d2** compound

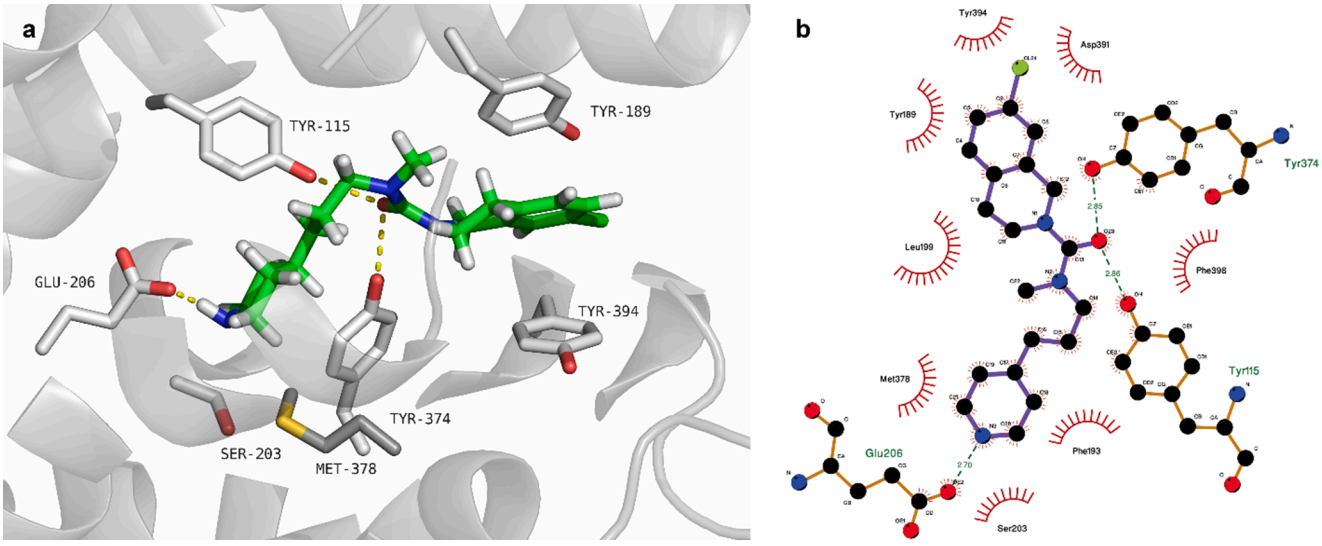

Fig. 3. **(a)** 3D representation of compound **d2** docked into the binding site of H_3R generated by PyMol program (version 1.7.x). The ligands and the main interacting residues are displayed as sticks. Only the side chains of the interacting residues from receptor are shown for further clarity. **(b)** 2D illustration of the interactions between compound **d2** and H_3R generated by LigPlot program.

as representative of all compounds docked into the binding site of H_3R. Analysis the docking results showed that the most important amino acids interact with H_3R are: Tyr^{115}, Tyr^{189}, Glu^{206}, Tyr^{374}, Met^{378}, Tyr^{394}. The predominant interactions observed for the selected molecules are: π-π stacking, ionic, and hydrogen bond interactions. The phenyl ring in hydrophobic/aromatic moiety of the compounds is engaged in π-π stacking with Tyr^{189} and Tyr^{394}. The ionic interaction is established between Glu^{206} and nitrogen of basic moiety. Tyr^{115} and Tyr^{374} make H-bonds with the linker (cf. Supplementary Fig. S4).

The best docked solution in complex with H_3R was subjected to a 50 ns molecular dynamics studies using AMBER package. Prior to proceed to binding free energy calculations, the stability of each system was evaluated based on conformational and energy analyses. Analysis of MD trajectory throughout the production period revealed that all the systems were adequately equilibrated and stable judged from calculated potential energy and root mean square deviation (RMSD) for each system (Supplementary Fig. S5). During the simulation period, the snapshots were extracted every 100 ps from the MD trajectory to be used for calculation of binding free energies using MM-PBSA/GBSA methodologies. The results of free energy values (ΔG) for ligand-receptor complexes can be found as Supplementary Table S6 online.

2.4. Chemistry

The synthesis has been performed by straight forward procedure from the *boc*-protected amine **1**, which alcohol functionality was transformed into amine **3** via Mitsonobu reaction and hydrazinolysis. The amine was transformed into isocyanate **4** by reaction with triphosgene, and then this isocyanate was taken for a convenient coupling to the 7-chlorinated 1,2,3,4-tetrahydroisochinoline derivative. Deprotection, or methylation and then deprotection led to the proposed lead structures **7** and **9** (**d2**), respectively (Fig. 4).

3. Human histamine H_3 receptor *in-vitro* assay

The result of human H_3R *in-vitro* assay using [^{3}H]-N^{α}-methylhistamine revealed affinity of the selected compound **d2** to hH_3R in low micromolar range. The demethylated **d2** showed lower affinity to hH_3R. Displacement curves of normalized data and determined K_i-values of **d2**, demethylated **d2** and pitolisant (as reference) are shown in Fig. 5. In comparison to pitolisant affinity estimates of **d2** are about 2 log units lower.

4. Materials and methods

4.1. Molecular field-based scaffold hopping

Computationally guided fragment and bioisosteric replacement tool implemented in Spark program (version 10.5.6; Cresset®, Cambridgeshire, UK) [32,33] was employed for performing scaffold hopping analysis on two previously identified potential lead compounds [22]. To accomplish this purpose, the starting compounds were fragmented in different portions followed by iterative experiments for finding similar fragments in terms of shape, pharmacophoric features, hydrophobicity, and electronic properties in region of interest. Following the creation of

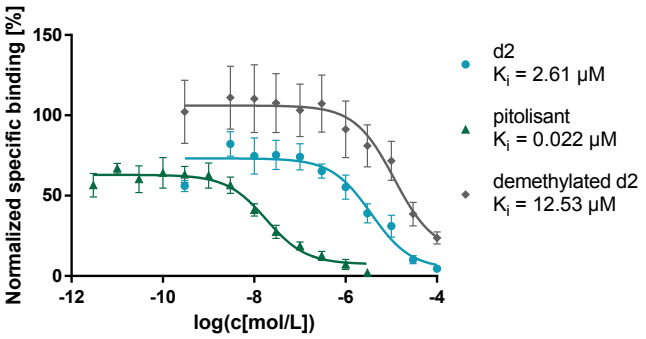

Fig. 5. Displacement of [^{3}H]-N^{α}-methylhistamine (**c** 2 nM, K_d = 3.08 nM) by **d2** (K_i = 2.61 [1.19–5.72] μM), demethylated **d2** (**7**) (K_i = 12.53 [4.79–32.76] μM) and pitolisant (K_i = 0.022 [0.002–0.250] μM). The assay were performed on HEK-293 cell membranes expressing the hH_3R. Data are expressed as mean values ± SEM (three independent experiments, each performed in duplicates).

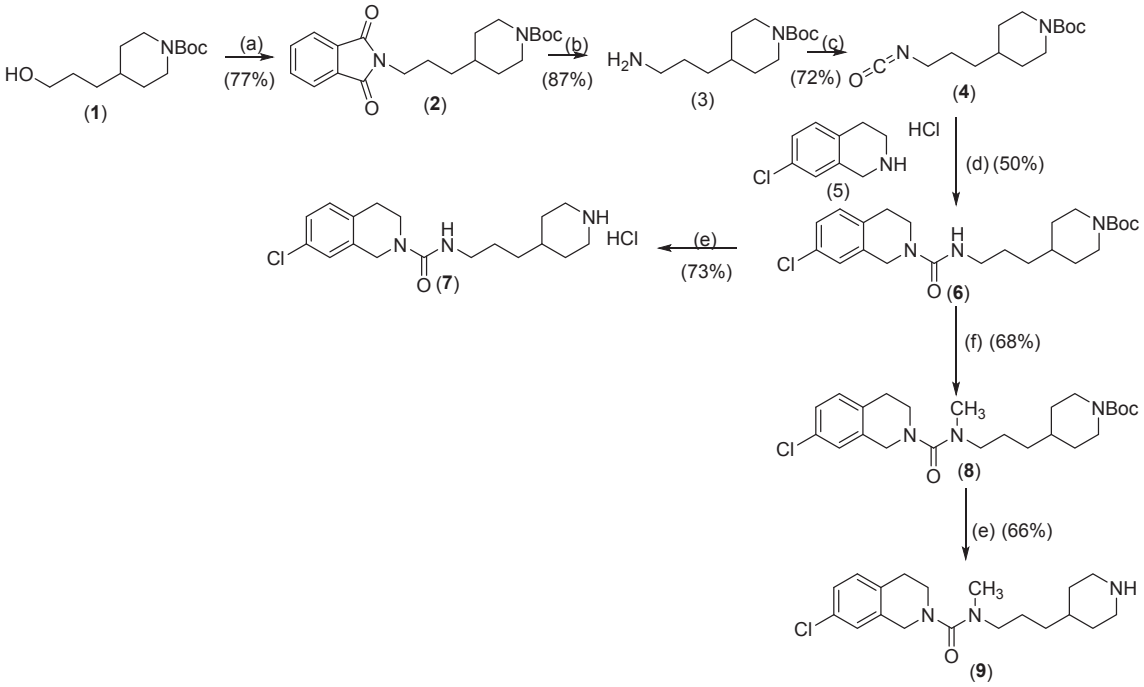

Fig. 4. Synthesis of compounds. Reagents and Conditions: (a) phthalimide, DEAD, PPh_3, THF; (b) hydrazine, EtOH; (c) triphosgene, sat. $NaHCO_3$, DCM; (d) DIPEA, DCM; (e) HCl sat. in dioxane; (f) NaH, MeI, THF;

the virtual library, the newly designed molecules were scored based on similarity of calculated fields to that of original compound.

4.2. In silico ADME and drug-likeness properties and toxicity assessment

The resulting compounds were comprehensively scrutinized according to the drug-likeness, ADME, and toxicity profiles. SwissADME web server (http://www.swissadme.ch) was used to compute physicochemical properties and predict pharmacokinetic and drug-likeness, and medicinal chemistry parameters [34]. Compounds fulfilled all the drug-likeness filtering criteria with desired ADME properties were selected for further evaluations. In addition, for predicting the potential target for the designed compounds in a chemical-pharmacological space, SwissTargetPrediction web server was employed [35]. In order to predict blood–brain barrier (BBB) permeability for the selected compounds, a drug-likeness central nervous system multiparameter optimization (CNS MPO) algorithm [31] proposed by Pfizer was applied. The CNS MPO score is calculated using the physiochemical parameters important for CNS drugs including: molecular weight (MW); lipophilicity as calculated partition coefficient (Clog P); calculated distribution coefficient at pH 7.4 (Clog D); ionization constant of the most basic center (pK_a) (ACD/Labs, version 6.00); topological polar surface area (TPSA) and number of hydrogen bond donors (HBDs). For calculation of ClogP, Bio-Loom program (version 5, Biobyte®) and for computing Clog D and pK_a, ACD/Labs software (version 6.00) were utilized. For toxicity assessment, off-target binding affinity profile of the candidate molecules were evaluated using OpenVirtualToxLab platform (version 5.8) [36,37]. In this platform, a thermodynamic-dependent parameter known as toxic potential (TP) is determined based on the flexible docking of a given query to 16 validated off-target proteins using 4D Boltzmann scoring criterion calculated for ligand-receptor complexes. The target proteins consist of nuclear receptors (androgen receptor (AR), estrogen receptor α (ERα), ERβ, glucocorticoid receptor (GR), mineralocorticoid receptor (MR), progesterone receptor (PR), liver X receptor (LXR), peroxisome proliferator-activated receptor γ (PPARγ), thyroid receptor α (TRα), and TRβ, cytochrome P450 enzyme family (1A2, 2C9, 2D6, 3A4), cytosolic transcription factor (aryl hydrocarbon receptor (AhR)) and potassium ion channel (hERG).

4.3. Molecular docking and binding free energy calculation studies

Following inspection of the designed compounds in terms of drug-likeness, ADME, CNS penetrability properties, and toxicity assessment, the candidate molecules were subjected to molecular docking experiment according to the procedure described previously [22]. Briefly, molecular docking of the retrieved compounds into the previously modeled structure of the H_3R [22] was conducted on a LINUX operating environment using GOLD program (version 5.0; CCDC Inc., Cambridge, UK) [38,39]. For defining the binding site, a geometric center was assigned based on the important amino acids involved in the binding pocket and all atoms in a 10 Å radius around the geometric center was set as the binding site of molecular docking. Moreover, two sets of distance constraints (1.5–3.5 Å) consisting of Tyr^{189} and Glu^{206} residues in H_3R model were applied in order to simulate the π-π stacking and ionic interactions observed for pitolisant structure [22]. For π-π stacking, phenyl groups of Tyr^{189} and designed compounds are considered whereas in the case of ionic interaction, electrostatic interaction between oppositely charged oxygen atom from Glu^{206} and nitrogen atom of piperidine/pyrrolidine ring from the designed molecules were imposed. During the semi-flexible protein–ligand docking calculations, the residues side chains engaged in the calculations were permitted to be flexible whereas the backbone atoms were considered rigid. Finally, the best docking pose among the solutions was selected on the basis of GoldScore fitness function and processed for molecular dynamics (MD) simulation analysis.

All the MD calculations were executed by Assisted Model Building with Energy Refinement (AMBER) package (version 14) [40,41] operating on a Linux-based (CentOS-6.8) GPU workstation consisting of four NvidiaK40M (each has 12 GB RAM and 2880 cuda cores), 2X Intel Xeon E5–2697 v2, 2.7 GHz (total of 48 cores), total RAM = 128 GB. The coordinate files for all ligands, protein, as well as ligand–protein complexes were generated by antechamber and LEaP module of AMBER. The FF14SB and GAFF force fields were applied for parameterization of protein and ligand, respectively. Then, the appropriate number of counter ions was added to electrostatically neutralize the total charge of the system. The neutralized complex was solvated using a rectangular box of explicit TIP3P water with buffering distance of 12 Å from the periphery of complex. Prior to MD simulation, different steps of minimization, heating, and equilibration were performed using Sander module of AMBER. Initially, energy minimization of solvated system was performed using 500 steps of steepest descent method followed by 500 steps of conjugate gradient algorithm. Afterwards, the system was gradually heated up from 0 to 300 K for 50 ps with subsequent 50 ps density equilibration at 300 K. The final equilibration of the system was conducted under constant pressure at 300 K for 500 ps using a 2 fs time step.

By applying SHAKE algorithm, all bonds involving hydrogen atoms were constrained. The SHAKE algorithm was employed to constrain all the bond lengths involving hydrogen atoms. Furthermore, a final 50 ns MD production was carried out by applying Particle Mesh Ewald (PME) method to treat long-range electrostatics interactions using GPU version of the PMEMD program. Periodic boundary conditions were used for all MD calculations without utilizing any constraint to either the ligand or the protein molecules. The simulation trajectory was obtained by capturing the coordinates every 10 ps during 50 ns of production period. Following the MD simulation, postprocessing of the trajectory was conducted using CPPTRAJ module implemented in AMBER. Moreover, the trajectory was also analyzed for calculation of binding free energy using Molecular Mechanics Poisson-Boltzmann Surface Area (MM-PBSA)/Generalized-Born Surface Area (GBSA) available in AMBER package [40,42]. Binding free energy for ligand–protein complexes was determined by summing up molecular mechanics energies, solvation-free energies, and entropic terms followed by averaging over the extracted equilibrated snapshots derived from MD simulation trajectory and presented as the average value. During the calculation of interaction energy, water molecules and counter ions were excluded. The interior and exterior dielectric constant was set to 1.0 and 80 for solute and the surrounding solvent, respectively.

Binding free energy ($\Delta G_{binding}$) is calculated according to the following equation:

$$\Delta G_{binding} = G_{water(complex)} - [G_{water(protein)} + G_{water(ligand)}] \quad (1)$$

where the terms denoted by $G_{water(complex)}$, $G_{water(protein)}$ and $G_{water(ligand)}$ refer to free energies of complex, protein, and ligand, respectively. Free energy for each species is obtained based on the following equations:

$$G = E_{gas} + G_{solvation} - TS \quad (2)$$

$$E_{gas} = E_{int} + E_{vdw} + E_{elec} \quad (3)$$

$$E_{int} = E_{bond} + E_{angle} + E_{torsion} \quad (4)$$

$$G_{solvation} = G_{polar} + G_{non-polar} \quad (5)$$

In the above equations, G demonstrates the calculated average free energy, E_{gas} shows the standard force-field energy, $G_{solvation}$ indicates solvation free energy and TS is vibrational entropy term. E_{gas} consists of internal strain energy (E_{int}) in the gas phase, non-covalent van der Waals (E_{vdw}) and electrostatic (E_{elec}) energies. The E_{int} consists of strain energies caused by deviation of the bonds (E_{bond}), angle (E_{angle}), and torsion angles (E_{tors}) from their equilibrium values. G_{polar} and $G_{non\text{-}polar}$ represent the polar and non-polar contributions to the solvation free

energy. The polar contribution is obtained from Poisson-Boltzmann or Generalized Born model whereas the non-polar contributions are determined by the calculation of solvent accessible surface area (SASA) based on the linear combinations of pairwise overlaps (LCPO) method [43]. In this work, the entropy contribution of the solute was ignored by considering similar solute entropy contribution on binding free energy for all the complexes.

4.4. Synthesis procedure

All starting materials have been obtained from Acros Organics (Geel, Belgium), Apollo Scientific (Cheshire,UK), Sigma Aldrich (part of Merck KGa Group, Darmdstadt, Germany), VWR (Darmstadt, Germany), and were used without further purification. Sorbent: Kieselgel 60 (0.04–0.063 mm) for column chromatography (Macherey-Nagel, Düren, Deutschland, Acros Organics, Geel, Belgien). Flash chromatography: Biotage Isolera™ Spektra Systems with *ACI*™ and Assist (Biotage, Uppsala, Sweden Stationary phase: Sfaer Silica D (Biotage, Uppsala, Sweden). Column capacity: 10 g, 25 g, 50 g, 100 g. Mass spectra have been determined using Advion Mass Express (Advion, Ithaca, USA). The expression CMS uses Edwards RV12 rotary vane pump and The CETAC ASX-7000 auto-sampler platform. Atmospheric-pressure chemical ionization (APCI) (constant current 0 – 15 μA) and electrospray ionization (ESI) (constant voltage 0 – 5 kV) were used as a method of ionization, operating in both positive and negative mode. Data have been shown as $[M + H^+]^+$. And $[M-H^+]^-$ Footprint - Width: 27 cm (10.6 in); Depth: 54.9 cm (21.6 in) rate range: Expression CMS :10 μL/min to 0.5 mL/min (ESI), 10 μL/min to 1.0 mL/min (APCI), nebulization gas: 0.5 L/mi, heated desolvation/APCI gas: 1 to 10 L/min. Mass calibration stability of ± 0.1 Da over the defined mass range (10 – 1200 for S systems and 10–2000 for L systems) over 12 h. Linear dynamic range of 5×10^3 The abundance of naturally occurring isotopes is accurately produced from the full-scan mass spectra. The expression CMS system Voltage: 100–240 VA, Frequency: 50–60 Hz CMS Fuse: 6 Amps, Max Power Consumption: 600 VA. NMR Spectroscopy: ^{1}H and ^{13}C NMR spectra of compounds of interest were measured at Bruker Avance III − 300 (Year 2010) and Bruker Avance III − 600 (Year 2011) Bruker, Germany. As NMR solvents were used $CDCl_3$ and DMSO-d_6 and tetramethylsylane was used as a standard.. Chemical shifts are given as parts per million (ppm) and been reported as: s (singlet), brs (broaden singulet), d (doublet), dd (double of doublets), ddd (double of double of doublets), dt (double of triplets), t (triplet), q(quartet), quint(quintet) or m (multiplet), Coupling constant (*J*) were given in Hertz (Hz).

Compounds purity was determined by liquid chromatography-mass spectrometry (LC-MS) Elute SP (HPG 700) Bruker Daltronics and amaZon speed ion Trap LC/MSn System (ESI-MS), Method: Alternating ion-Polarity :on; Scan Range: *m/z*: 80–1200; Nebulizer: Nitrogen, 15 Psi; Dry Gas: Nitrogen, 8 L/min, 200 °C; Massrange Mode: UltraScan; Column: Intensity Solo 2 C18 (100 mm * 2.1 mm); Temperature: 50 °C; Mobile phase: A. water hypergrade for LC-MS with 0.1 % formic acid (v/v) (Merck); B. Acetonitrile hypergrade for LC-MS (for LC-MS); Method of Analysis: 0–4 min 98 % A, 4–5 min gradient 95% A, 5–9 min 95 % A, 9–16 min gradient 5% A, 16–17 min. gradient to 0% A, reconditioning: 17–18 min. gradient to 98 % A, 18–21 min 98 % A.

Synthetic route started using Mitsunobu reaction of compound (1) and phtalimide . Resulting compound (2) was deprotected to amine with hydrazine under reflux in ethanol [44]. Free amine, after derivatisation to isocyanate (4) [45] reacted with compound (5) in THF to form urea compound (6). Methylation of (6) afforded after deprotection of Boc compound **d2** (**9**). Deprotection of compound (**6**) afforded demethylated compound **d2** (**7**) [46].

4.4.1. *tert-Butyl 4-(3-(1,3-dioxoisoindolin-2-yl)propyl)piperidine-1-carboxylate (2) [44]*

To a solution of *tert*-butyl 4-(3-hydroxypropyl)piperidine-1-carboxylate (1) (1.2 g, 4.9 mmol) and phthalimide (1.2 eq., 880 mg, 6.0 mmol) in THF (20 mL) was added PPh_3 (1.5 eq., 1.9 g, 7.3 mmol) and DEAD (1.5 eq. 1.27 g, 7.3 mmol) at RT. The resulting mixture was stirred at RT overnight and diluted with EtOAc (100 mL) . The organic layer was washed with brine (20 mL × 2) and dried over anhydrous $MgSO_4$. The organic phase was concentrated and the residue was purified by flash chromatography (hexane/EtOAc 3/1) to afford *tert*-butyl 4- (3- (1, 3-dioxoisoindolin-2-yl) propyl) piperidine-1-carboxylate (1.41 g, 77 %) ; APCI *m/z* (-): 372,6 ($[M-H^+]^-$); ^{1}H NMR: δ [ppm] (300 MHz, DMSO-d_6) δ 8.00–7.70 (m, 4H), 3.90 (d, J = 13.1 Hz, 2H), 3.55 (t, J = 7.1 Hz, 2H), 2.64 (m, 2H), 1,70–1,50 (m, 4H), 1,37 (s, 9H), 1.25–1.05 (m, 3H), 0.92 (qd, J = 12.5 Hz, 4.3 Hz, 2H);

4.4.2. *tert-Butyl 4- (3-aminopropyl) piperidine-1-carboxylate (3) [44]*

To a solution of *tert*-butyl 4- (3- (1, 3-dioxoisoindolin-2-yl) propyl) piperidine-1-carboxylate (2) (1.41 g, 3.8 mmol) in 25 mL EtOH was added 60 % hydrazine hydrate (3 mL) . The mixture was stirred at reflux for 3 h and then the solid was filtered off. The filtrate was concentrated under reduced pressure and the residue was suspended in DCM (50 mL) and filtered. The filtrate was concentrated to give the crude *tert*-butyl 4-(3-aminopropyl) piperidine-1-carboxylate (800 mg, 95) which was used in next step directly. Yield (800 mg, 87 %); APCI *m/z*(+): $[(M + H^+)]^+$ 243.3; ^{1}H NMR: δ [ppm] (300 MHz, DMSO-d_6) δ 3.90 (d, J = 13.1 Hz, 2H), 3.40 (bs, 2H), 2.65 (m, 2H), 2.50 (m, 2H), 1,60(m, 2H), 1,37 (m, 12H), 1.25–1.05 (m, 2H), 0.92 (qd, J = 12.5 Hz, 4.3 Hz, 2H);

4.4.3. *tert-Butyl 4-(3-isocyanatopropyl)piperidine-1-carboxylate (4) [45]*

To a vigorously stirred mixture of *tert*-butyl 4- (3-aminopropyl) piperidine-1-carboxylate (3) (400 mg, 1.65 mmol) in DCM (6 mL) and saturated $NaHCO_3$ (6 mL), cooled at 0 °C was added triphosgene (490 mg, 1.65 mmol). After 1 h at 0 °C the mixture was diluted with DCM and the layers were separated. Organic layer was dried over $MgSO_4$ and evaporated to dryness. Yield (320 mg, 72 %); APCI *m/z*(+): $[(M + H^+)]^+$ 269.3; ^{1}H NMR: δ [ppm] (300 MHz, DMSO-d_6) δ 3.98 (d, J = 13.0 Hz, 2H), 2.74 (m, 2H), 1.63 (m, 4H), 1.45 (s, 10*H*), 1.37 – 1.20 (m, 2H), 1.01 (qd, J = 12.4, 4.3 Hz, 2H).

4.4.4. *tert-Butyl 4-(3-(7-chloro-1,2,3,4-tetrahydroisoquinoline-2-carboxamido)propyl)piperidine-1-carboxylate **(6)** [46,47]*

tert-Butyl 4-(3-isocyanatopropyl)piperidine-1-carboxylate (4) (180 mg, 0.7 mmol), DIPEA (1.2 eq, 1.1 mmol, 188 μL) and 7-chloro-1,2,3,4-tetrahydroisoquinoline hydrochloride (5) (0.9 mmol, 150 mg) were dissolved in 20 mL of THF and stirred at RT over 48 h. The reaction mixture was evaporated to dryness and portioned between DCM (50 mL) and water (30 mL). Water layer was extracted with DCM twice more. Collected organic layers were dried over MgSO4 and the residue was purified by silica gel chromatography (hexane/EtOAc 1/3) to afford *tert*-butyl 4-(3-(7-chloro-1,2,3,4-tetrahydroisoquinoline-2-carboxamido) propyl)piperidine-1-carboxylate (146 mg, 50 %); APCI *m/z*(+): $[(M + H^+)]^+$ 437.1; ^{1}H NMR:δ [ppm] (300 MHz, DMSO-d_6) δ 7.28–6.97 (m, 3H), 6.53 (t, J = 5.4 Hz, 1H), 4.44 (s, 2H), 3.88 (d, J = 13.1 Hz, 2H), 3.49 (t, J = 5.9 Hz, 2H), 2.99 (q, J = 6.8 Hz, 2H), 2.78–2.52 (m, 4H), 1.97 (s, 2H), 1.59 (s, 2H), 1.36 (s, 12H), 1.01–0.77 (m, 2H);

4.4.5. *7-Chloro-N-(3-(piperidin-4-yl)propyl)-3,4-dihydroisoquinoline-2 [1H]-carboxamide hydrochloride **(7)***

tert-Butyl-4-(3-(7-chloro-1,2,3,4-tetrahydroisoquinoline-2-carboxamido)propyl)piperidine-1-carboxylate (**6**) (140 mg, 0.33 mmol) was dissolved in 2 mL of saturated HCl solution in dioxane and left stirring for 1 h. Reaction mixture was coevaporated a three times with dioxane. The crude product was washed with Et_2O to afford pure 7-chloro-*N*-(3-(piperidin-4-yl)propyl)-3,4-dihydroisoquinoline-2[1*H*]-carboxamide hydrochloride (90 mg, 73 %); APCI *m/z*(+): $[(M + H^+)]^+$ 336.2; ^{1}H NMR: δ [ppm] (300 MHz, DMSO-d_6) δ 8.95 (bs, 2H), 7.31–7.05 (m, 3H), 6.64 (s, 1H), 4.47 (s, 2H), 3.49 (t, J = 7.1 Hz, 2H), 3.29–3.10(m, 2H), 3.01 (t, J = 7.1 Hz, 2H), 2.88–2.66 (m, 4H), 1.89–1.65 (m, 2H), 1,54–1.05 (m, 7H);); 13C NMR (75 MHz, DMSO-d_6) δ 157.23, 136.68,

133.80, 130.41, 130.22,126.04, 125.82, 60.68, 45.03, 43.03, 40.85, 40.16, 39.05, 32.78, 29.16, 28.30, 27.48; LC-MS (ESI-(+)): 95.3 % 336.09 $[M + H^+]^+$;

4.4.6. *tert-Butyl-4-(3-(7-chloro-N-methyl-1,2,3,4-tetrahydroisoquinoline-2-carboxamido)propyl)piperidine-1-carboxylate* (**8**) [46]

tert-Butyl 4-(3-(7-chloro-1,2,3,4-tetrahydroisoquinoline-2-carboxamido)propyl)piperidine-1-carboxylate (**6**) (250 mg, 0.57 mmol) was dissolved in 30 mL of THF and excess of NaH (60 % on oil, 100 mg) was added). The reaction mixture was allowed to stir at RT for 3 h. After three hours an excess of methyl iodide (5.0 mL) was added and the stirring was continued over night). Reaction mixture was evaporated to dryness and purified by flash chromatography (hexane/EtOAc, 1/3) to afford *tert*-butyl 4-(3-(7-chloro-*N*-methyl-1,2,3,4-tetrahydroisoquinoline-2-carboxamido)propyl)piperidine-1-carboxylate (173 mg, 68 %). APCI *m/z*(+): $[(M + H^+)]^+$ 450.3; ^{1}H NMR: δ [ppm] (300 MHz, DMSO-d_6) δ 7.30–7.12 (m, 3H), 4.27 (s, 2H), 3.89 (d, $J = 13.1$ Hz, 2H), 3.40–3.32 (m, 2H),3.11 (t, $J = 7.3$ Hz, 2H), 2.80 (m, 5H), 2.61 (m, 2H), 1.54 (m, 3H), 1.38 (s, 9H), 1.24 (s, 2H) , 1.13 (m, 2H), 1.01–0.79 (m, 2H);

4.4.7. *7-Chloro-N-methyl-N-(3-(piperidin-4-yl)propyl)-3,4-dihydroisoquinoline-2[1H]-carboxamide* (**9**)

tert-Butyl-4-(3-(7-chloro-*N*-methyl-1,2,3,4-tetrahydroisoquinoline-2-carboxamido)propyl)piperidine-1-carboxylate (**8**) (200 mg, 0.44 mmol) was dissolved in 4 mL of saturated HCl solution in dioxane and left stirring for 1 h. Reaction mixture was coevaporated a three times with dioxane. The crude product was purified by column chromatography (DCM/MeOH (sat·NH_3) 95/5) to afford (9): (102 mg, 66 %). APCI *m/z*(+): $[(M + H^+)]^+$ 351.0; ^{1}H NMR: δ [ppm] (300 MHz, $CDCl_3$) δ 7.17–6.84 (m, 3H), 4.26 (s, 2H), 3.37 (t, $J = 5.8$ Hz, 2H), 3.11 (t, $J = 7.5$ Hz, 2H), 2.93 (d, $J = 10.4$ Hz, 2H), 2.79 (d, $J = 2,4$ Hz, 6H), 2.05–1.71 (m, 2H), 1.65–0.98 (m, 9H); ^{13}C NMR (75 MHz, $CDCl_3$) δ 164.65, 135.82, 133.01, 131.62, 130.17, 126.54, 126.21, 53.44, 50.34, 48.61, 44.87, 44.41, 36.51, 36.26, 35.63, 33.50, 31.90, 28.14, 24.24 ; LC-MS (ESI-(+)): 95.1 % 336.09 $[M + H^+]^+$;

4.5. *Human histamine H_3 receptor in-vitro assay*

Compounds were tested in H_3R binding studies *in-vitro* as reported previously [48] Click or tap here to enter text.. Briefly summarized, crude hH_3R membrane extracts from HEK-293 cells stably expressing the hH_3R were incubated with several concentrations of test compounds and [^{3}H]-N^{α}-methylhistamine (2 nM, $K_D = 3.08$ nM). The cell line was kind gift from Prof. J.-C. Schwartz, Bioprojet Pharma, France. Non-specific binding was determined using pitolisant (10 μM final concentration). Obtained data in duplicates from at least three independent experiments were analyzed with GraphPad Prism 7 (San Diego, CA, USA) using non-linear regression. K_i values were transformed from IC_{50} according to Cheng-Prusoff [49]. Statistical analysis of pK_i values was performed and converted to mean K_i values and 95% confidence intervals.

5. Discussion

According to the profound impact of histamine H_3 receptors in modulating the release of histamine and other important neurotransmitters in central nervous system, these receptors deserve much consideration as an important target in neurological disorders. Since neurotransmitter deficiency in CNS has been implicated in several neurological disorders, developing histamine H_3R antagonists/inverse agonists is of paramount importance in this line of research. Drug design and discovery pipeline is a multiobjective optimization process necessitates contribution of various disciplines. In view of this, computational approaches are inevitable part of pharmaceutical research accelerating the identification of novel therapeutic agents in early stages of rational drug design. Scaffold hopping technique as structural optimization strategy in medicinal chemistry aims to improve the key parameters of any bioactive compound in terms of safety and efficacy. In the current study, scaffold-hopping analysis was performed on previously identified compounds [22] to find potentially bioisosteric substructures with similar shape and electronic properties in order to develop novel molecules with improved pharmacokinetic and physicochemical attributes while simultaneously lacking of any potentially toxic fragments. For this purpose, a variety of scaffolds are shuffled based on the calculated field points. This replacement was noticeable especially for compound 3 containing indole and piperazine moieties reported as structural elements frequently observed in promiscuous compounds [50].

The newly designed molecules containing favorable bioisosteres with high similarity to the starter molecule were carefully scrutinized on the basis of BIF scores, radial plots, and unstable/reactive functional groups. The obtained candidate molecules were inspected in terms of drug-likeness, ADME, selectivity towards H_3R, and toxicity. The designed molecules were predicted to have high intestinal absorption. The majority of the candidates showed no inhibition of drug metabolizing isoforms of CYP450 enzymes. Moreover, no violation of rules determining drug-likeness were observed for the selected compounds. Since CNS penetration is essential for H_3R ligands, the calculated MPO score demonstrated the possible brain permeability for the designed compounds within the defined threshold. The off-target activity prediction for the selected compounds revealed lower potential of candidate molecules to be toxic. To predict the mode of interaction of the selected molecules with H_3R, molecular docking was conducted. Analysis the results indicate the key residues interact with different moieties of the candidate molecules are: Tyr^{189} (TM5) and Tyr^{394} (TM7) involved in hydrophobic interaction in hydrophobic/aromatic moiety, Tyr^{115} (TM3) and Tyr^{374} (TM6) interact with the linker, and Glu^{206} (TM5) in ionic interaction with basic moiety. The results are in agreement with the other investigations reported previously [51–58]. The results of binding free energy values (ΔG) for the designed molecules presented (cf. Supplementary Table S6) revealed that the binding affinity for the majority of them are lower compared to pitolisant implying the suitable predicted affinity of the designed compounds towards H_3R.

In the next step, compound **d2** was considered as a representative for the designed compounds for synthesis and affinity measurement. This compound has a high synthetically feasible structure associated with the necessary features considered for screening and is lacking any stereocenters. Moreover, among the compounds it is the only one that passed all the lead-likeness criteria. In addition, it possess the lowest TPSA in this set of compound proving the potential new lead structure.

In accordance with the results of binding free energy values, **d2** showed lower binding affinity in radioligand displacement assay to hH_3R than that of pitolisant. Demethylation into compound **7** led to decreased affinity. Although, experimental determined affinity of **d2** is not in the submicromolar K_i-range as previously identified compounds [22], binding affinities are in good agreement with molecular docking simulations and offer another scaffold for histamine H_3R antagonists [4,59,60].

6. Conclusion

Substantial progress in developing histamine H_3R antagonists/inverse agonists has been made in the past decades owing to the significant role of H_3 receptors in neurological diseases. In this investigation, we sought to identify novel H_3R antagonists by applying computational approaches integrated with experimental validation. For this purpose, scaffold-hopping technique was utilized to design novel compounds based on calculated field point patterns on previously identified H_3 antagonists using ChEMBL and Zinc database. Following the filtering the compounds on the basis of pharmacokinetic, drug-likeness and toxicity parameters, the selected compounds were subjected to molecular docking and dynamics simulation studies in order to predict the binding

mode and binding free energy estimation, respectively. Considering the predicted features as well as synthetic tractability of the designed compounds, **d2** compound was selected for synthesis. The biological evaluation using radioligand displacement study revealed micromolar K_i values for **d2** and its demethylated derivative. The presented novel histamine H_3 ligands with the new 1,2,3,4-tetrahydroisoquinoline element can provide a safe and promising framework for further optimization through medicinal chemistry oriented strategies.

Declaration of Competing Interest

The authors declare that they have no known competing financial interests or personal relationships that could have appeared to influence the work reported in this paper.

Acknowledgements

The authors thank to Biotechnology Research Center and School of Pharmacy, Tabriz university of Medical Sciences for providing computational resources (Grant No: 64123). Support by the EU COST Actions CA15135, CA18133, and CA18240 is greatly acknowledged (to HS).

Author contributions

NS and SKH carried out the computational simulations. AZ and LL performed the chemical synthesis and in vitro evaluations. SD helped in analyzing the results. MHM and HS designed the study, analyzed the data, supervised the project, and prepared the manuscript. All authors have read the manuscript and approved the final version.

Appendix A. Supplementary material

Supplementary data to this article can be found online at https://doi.org/10.1016/j.bioorg.2021.105411.

References

[1] G. Nieto-Alamilla, R. Márquez-Gómez, A.-M. García-Gálvez, G.-E. Morales-Figueroa, J.-A. Arias-Montaño, The Histamine H3 Receptor: Structure, Pharmacology, and Function, Mol. Pharmacol. 90 (5) (2016) 649–673, https://doi.org/10.1124/mol.116.104752.

[2] M.J. Gemkow, A.J. Davenport, S. Harich, B.A. Ellenbroek, A. Cesura, D. Hallett, The histamine H3 receptor as a therapeutic drug target for CNS disorders, Drug Discov. Today. 14 (9–10) (2009) 509–515, https://doi.org/10.1016/j.drudis.2009.02.011.

[3] M. Berlin, C.W. Boyce, M. de Lera Ruiz, Histamine H3 receptor as a drug discovery target, J. Med. Chem. 54 (1) (2011) 26–53, https://doi.org/10.1021/jm100064d.

[4] N. Ghamari, O. Zarei, J.-A. Arias-Montaño, D. Reiner, S. Dastmalchi, H. Stark, M. Hamzeh-Mivehroud, Histamine H3 receptor antagonists/inverse agonists: Where do they go? Pharmacol. Ther. 200 (2019) 69–84, https://doi.org/10.1016/j.pharmthera.2019.04.007.

[5] G. Sliwoski, S. Kothiwale, J. Meiler, E.W. Lowe, E.L. Barker, Computational methods in drug discovery, Pharmacol. Rev. 66 (1) (2014) 334–395, https://doi.org/10.1124/pr.112.007336.

[6] G. Schneider, P. Schneider, S. Renner, Scaffold-Hopping: How Far Can You Jump? QSAR Comb. Sci. 25 (12) (2006) 1162–1171, https://doi.org/10.1002/(ISSN)1611-021810.1002/qsar.v25:1210.1002/qsar.200610091.

[7] S.R. Langdon, P. Ertl, N. Brown, Bioisosteric Replacement and Scaffold Hopping in Lead Generation and Optimization, Mol. Inform. 29 (5) (2010) 366–385, https://doi.org/10.1002/minf.201000019.

[8] H.-J. Böhm, A. Flohr, M. Stahl, Scaffold hopping, Drug Discov. Today Technol. 1 (3) (2004) 217–224, https://doi.org/10.1016/j.ddtec.2004.10.009.

[9] Y.Y. Syed, Y. Pitolisant: First Global Approval, Drugs. 76 (13) (2016) 1313–1318, https://doi.org/10.1007/s40265-016-0620-1.

[10] M. Kollb-Sielecka, P. Demolis, J. Emmerich, G. Markey, T. Salmonson, M. Haas, The European Medicines Agency review of pitolisant for treatment of narcolepsy: summary of the scientific assessment by the Committee for Medicinal Products for Human Use, Sleep Med. 33 (2017) 125–129, https://doi.org/10.1016/j.sleep.2017.01.002.

[11] Z. Szakacs, Y. Dauvilliers, V. Mikhaylov, I. Poverennova, S. Krylov, S. Jankovic, K. Sonka, P. Lehert, I. Lecomte, J.-M. Lecomte, J.-C. Schwartz, M. Poluektov, E. Yakupov, A. Kalinkin, M. Aksu, H. Yilmaz, G. Benbir, D. Wolynczyk-Gmaj, W. Jernajczyk, I. Staykov, A.N. Tavarari, Safety and efficacy of pitolisant on cataplexy in patients with narcolepsy: a randomised, double-blind, placebo-controlled trial, Lancet Neurol. 16 (3) (2017) 200–207, https://doi.org/10.1016/S1474-4422(16)30333-7.

[12] H. Sun, C. MacLeod, K. Mostoller, C. Mahon, L. Han, J.J. Renger, J. Ma, K. R. Brown, V. Schulz, G.G. Kay, W.J. Herring, C. Lines, L.B. Rosen, M.G. Murphy, J. A. Wagner, Early-stage comparative effectiveness: randomized controlled trial with histamine inverse agonist MK-7288 in excessive daytime sleepiness patients, J. Clin. Pharmacol. 53 (12) (2013) 1294–1302, https://doi.org/10.1002/jcph.v53.1210.1002/jcph.182.

[13] J.R. Stokes, F.A. Romero, R.J. Allan, P.G. Phillips, F. Hackman, J. Misfeldt, T. B. Casale, The effects of an H3 receptor antagonist (PF-03654746) with fexofenadine on reducing allergic rhinitis symptoms, J. Allergy Clin. Immunol. 129 (2) (2012) 409–412.e2, https://doi.org/10.1016/j.jaci.2011.11.026.

[14] O. Spiegelstein, et al., Pharmacokinetics, pharmacodynamics and safety of CEP-26401, a high-affinity histamine-3 receptor antagonist, following single and multiple dosing in healthy subjects, J. Psychopharmacol. 30 (2016) 983–993.

[15] C.J. Schwartzbach, et al., Lesion remyelinating activity of GSK239512 versus placebo in patients with relapsing-remitting multiple sclerosis: a randomised, single-blind, phase II study, J. Neurol. 264 (2017) 304–315.

[16] A.A. Othman, et al., The H3 antagonist ABT-288 is tolerated at significantly higher exposures in subjects with schizophrenia than in healthy volunteers, Br. J. Clin. Pharmacol. 77 (2014) 965–974.

[17] P.J. Nathan, et al., The safety, tolerability, pharmacokinetics and cognitive effects of GSK239512, a selective histamine H(3) receptor antagonist in patients with mild to moderate Alzheimer's disease: a preliminary investigation, Curr. Alzheimer Res. 10 (2013) 240–251.

[18] Jucaite, A. et al. AZD5213: a novel histamine H3 receptor antagonist permitting high daytime and low nocturnal H3 receptor occupancy, a PET study in human subjects. Int. J. Neuropsychopharmacol. 16, 1231-1239, 10.1017/s1461145712001411 (2013).

[19] Dauvilliers, Y. et al. Pitolisant versus placebo or modafinil in patients with narcolepsy: a double-blind, randomised trial. Lancet Neurol. 12, 1068-1075, 10.1016/S1474-4422(13)70225-4 (2013).

[20] P. Daley-Yates, et al., The efficacy and tolerability of two novel H(1)/H(3) receptor antagonists in seasonal allergic rhinitis, Int. Arch. Allergy Immunol. 158 (2012) 84–98, https://doi.org/10.1159/000329738.

[21] S. Ashworth, A. Berges, E.A. Rabiner, A.A. Wilson, R.A. Comley, R.Y.K. Lai, R. Boardley, G. Searle, R.N. Gunn, M. Laruelle, V.J. Cunningham, Unexpectedly high affinity of a novel histamine H3 receptor antagonist, GSK239512, in vivo in human brain, determined using PET, Br. J. Pharmacol. 171 (5) (2014) 1241–1249, https://doi.org/10.1111/bph.12505.

[22] N. Ghamari, O. Zarei, D. Reiner, S. Dastmalchi, H. Stark, M. Hamzeh-Mivehroud, Histamine H3 receptor ligands by hybrid virtual screening, docking, molecular dynamics simulations, and investigation of their biological effects, Chem. Biol. Drug Des. 93 (5) (2019) 832–843, https://doi.org/10.1111/cbdd.2019.93.issue-510.1111/cbdd.13471.

[23] N. Ghamari, S. Dastmalchi, O. Zarei, J.-A. Arias-Montaño, D. Reiner, F. Ustun-Alkan, H. Stark, M. Hamzeh-Mivehroud, In silico and in vitro studies of two non-imidazole multiple targeting agents at histamine H3 receptors and cholinesterase enzymes, Chem. Biol. Drug Des. 95 (2) (2020) 279–290, https://doi.org/10.1111/cbdd.v95.210.1111/cbdd.13642.

[24] C.A. Lipinski, F. Lombardo, B.W. Dominy, P.J. Feeney, Experimental and computational approaches to estimate solubility and permeability in drug discovery and development settings, Adv. Drug Deliv. Rev. 46 (2001) 3–26.

[25] A.K. Ghose, V.N. Viswanadhan, J.J. Wendoloski, A Knowledge-Based Approach in Designing Combinatorial or Medicinal Chemistry Libraries for Drug Discovery. 1. A Qualitative and Quantitative Characterization of Known Drug Databases, J. Comb. Chem. 1 (1999) 55–68.

[26] W.J. Egan, K.M. Merz Jr., J.J. Baldwin, Prediction of drug absorption using multivariate statistics, J. Med. Chem. 43 (2000) 3867–3877.

[27] I. Muegge, S.L. Heald, D. Brittelli, Simple Selection Criteria for Drug-like Chemical Matter, J. Med. Chem. 44 (2001) 1841–1846.

[28] D.F. Veber, et al., Molecular properties that influence the oral bioavailability of drug candidates, J. Med. Chem. 45 (2002) 2615–2623.

[29] J.B. Baell, G.A. Holloway, New Substructure Filters for Removal of Pan Assay Interference Compounds (PAINS) from Screening Libraries and for Their Exclusion in Bioassays, J. Med. Chem. 53 (7) (2010) 2719–2740, https://doi.org/10.1021/jm901137j.

[30] R. Brenk, A. Schipani, D. James, A. Krasowski, I. Gilbert, J. Frearson, P. Wyatt, Lessons Learnt from Assembling Screening Libraries for Drug Discovery for Neglected Diseases, ChemMedChem. 3 (3) (2008) 435–444, https://doi.org/10.1002/(ISSN)1860-718710.1002/cmdc.v3:310.1002/cmdc.200700139.

[31] T.T. Wager, X. Hou, P.R. Verhoest, A. Villalobos, Moving beyond rules: the development of a central nervous system multiparameter optimization (CNS MPO) approach to enable alignment of druglike properties, ACS Chem. Neurosci. 1 (6) (2010) 435–449, https://doi.org/10.1021/cn100008c.

[32] T. Cheeseright, M. Mackey, S. Rose, A. Vinter, Molecular Field Extrema as Descriptors of Biological Activity: Definition and Validation, J. Chem. Inf. Model. 46 (2006) 665–676, https://doi.org/10.1021/ci050357s.

[33] P.H. Olesen, The use of bioisosteric groups in lead optimization, Curr. Opin. Drug Discov. Devel. 4 (2001) 471–478.

[34] A. Daina, O. Michielin, V. Zoete, SwissADME: a free web tool to evaluate pharmacokinetics, drug-likeness and medicinal chemistry friendliness of small molecules, Sci. Rep. 7 (2017) 42717, https://doi.org/10.1038/srep42717.

[35] A. Daina, O. Michielin, V. Zoete, SwissTargetPrediction: updated data and new features for efficient prediction of protein targets of small molecules, Nucleic Acids Res. 47 (2019) W357–W364, https://doi.org/10.1093/nar/gkz382.

[36] A. Vedani, M. Dobler, Z. Hu, M. Smieško, OpenVirtualToxLab–a platform for generating and exchanging in silico toxicity data, Toxicol. Lett. 232 (2) (2015) 519–532, https://doi.org/10.1016/j.toxlet.2014.09.004.
[37] A. Vedani, M. Dobler, M. Smiesko, VirtualToxLab - a platform for estimating the toxic potential of drugs, chemicals and natural products, Toxicol. Appl. Pharmacol. 261 (2012) 142–153.
[38] G. Jones, P. Willett, R.C. Glen, Molecular recognition of receptor sites using a genetic algorithm with a description of desolvation, J. Mol. Biol. 245 (1995) 43–53.
[39] G. Jones, P. Willett, R.C. Glen, A.R. Leach, R. Taylor, Development and validation of a genetic algorithm for flexible docking, J. Mol. Biol. 267 (1997) 727–748, https://doi.org/10.1006/jmbi.1996.0897.
[40] D.A. Case, et al., The Amber biomolecular simulation programs, J. Comput. Chem. 26 (2005) 1668–1688.
[41] D.A. Pearlman, D.A. Case, J.W. Caldwell, W.S. Ross, T.E. Cheatham, S. DeBolt, D. Ferguson, G. Seibel, P. Kollman, AMBER, a package of computer programs for applying molecular mechanics, normal mode analysis, molecular dynamics and free energy calculations to simulate the structural and energetic properties of molecules, Comput. Phys. Commun. 91 (1-3) (1995) 1–41, https://doi.org/10.1016/0010-4655(95)00041-D.
[42] P.A. Kollman, et al., Calculating structures and free energies of complex molecules: combining molecular mechanics and continuum models, Acc. Chem. Res. 33 (2000) 889–897, https://doi.org/10.1021/ar000033j.
[43] J. Weiser, S. Shenkin Peter, W.C. Still, Approximate atomic surfaces from linear combinations of pairwise overlaps (LCPO), J. Comput. Chem. 20 (1999) 217–230, https://doi.org/10.1002/(SICI)1096-987X(19990130)20:2<217::AID-JCC4>3.0.CO;2-A.
[44] Rudd, M. T. et al. N-Aryl and N-Heteroaryl Piperidine Derivatives As Liver X Receptor B Agonists, Compositions, and Their Use. WO2018/68297 (2018).
[45] P. Trivedi, N. Adhikari, S.A. Amin, Y. Bobde, R. Ganesh, T. Jha, B. Ghosh, Design, synthesis, biological evaluation and molecular docking study of arylcarboxamido piperidine and piperazine-based hydroxamates as potential HDAC8 inhibitors with promising anticancer activity, Eur. J. Pharm. Sci. 138 (2019) 105046, https://doi.org/10.1016/j.ejps.2019.105046.
[46] R. Bach, J. Clayden, U. Hennecke, A-Arylation of Cyclic Amines by Aryl Transfer in Lithiated Ureas, SYNLETT 03 (2009) 421–424.
[47] S. Del Prete, V. De Luca, C. Capasso, C.T. Supuran, V. Carginale, Recombinant thermoactive phosphoenolpyruvate carboxylase (PEPC) from Thermosynechococcus elongatus and its coupling with mesophilic/thermophilic bacterial carbonic anhydrases (CAs) for the conversion of CO2 to oxaloacetate, Bioorg. Med. Chem. 24 (2) (2016) 220–225, https://doi.org/10.1016/j.bmc.2015.12.005.
[48] M.A. Khanfar, D. Reiner, S. Hagenow, H. Stark, Design, synthesis, and biological evaluation of novel oxadiazole- and thiazole-based histamine H(3)R ligands, Bioorg. Med. Chem. 26 (14) (2018) 4034–4046, https://doi.org/10.1016/j.bmc.2018.06.028.
[49] C. Yung-Chi, W.H. Prusoff, Relationship between the inhibition constant (KI) and the concentration of inhibitor which causes 50 per cent inhibition (I50) of an enzymatic reaction, Biochem. Pharmacol. 22 (23) (1973) 3099–3108, https://doi.org/10.1016/0006-2952(73)90196-2.
[50] N.A. Meanwell, Improving drug candidates by design: a focus on physicochemical properties as a means of improving compound disposition and safety, Chem. Res. Toxicol. 24 (9) (2011) 1420–1456, https://doi.org/10.1021/tx200211v.
[51] F.U. Axe, S.D. Bembenek, S. Szalma, Three-dimensional models of histamine H3 receptor antagonist complexes and their pharmacophore, J. Mol. Graph. Model. 24 (2006) 456–464.
[52] M. Bajda, K.J. Kuder, D. Łażewska, K. Kieć-Kononowicz, A. Więckowska, M. Ignasik, N. Guzior, J. Jończyk, B. Malawska, Dual-acting diether derivatives of piperidine and homopiperidine with histamine H(3) receptor antagonistic and anticholinesterase activity, Arch. Pharm. (Weinheim) 345 (8) (2012) 591–597, https://doi.org/10.1002/ardp.v345.810.1002/ardp.201200018.
[53] S. Harusawa, K. Sawada, T. Magata, H. Yoneyama, L. Araki, Y. Usami, K. Hatano, K. Yamamoto, D. Yamamoto, A. Yamatodani, Synthesis and evaluation of N-alkyl-S-[3-(piperidin-1-yl)propyl]isothioureas: high affinity and human/rat species-selective histamine H(3) receptor antagonists, Bioorg. Med. Chem. Lett. 23 (23) (2013) 6415–6420, https://doi.org/10.1016/j.bmcl.2013.09.052.
[54] K. Kuder, D. Łażewska, G. Latacz, J.S. Schwed, T. Karcz, H. Stark, J. Karolak-Wojciechowska, K. Kieć-Kononowicz, Chlorophenoxy aminoalkyl derivatives as histamine H(3)R ligands and antiseizure agents, Bioorg. Med. Chem. 24 (2) (2016) 53–72, https://doi.org/10.1016/j.bmc.2015.11.021.
[55] D. Łażewska, J. Jończyk, M. Bajda, N. Szałaj, A. Więckowska, D. Panek, C. Moore, K. Kuder, B. Malawska, K. Kieć-Kononowicz, Cholinesterase inhibitory activity of chlorophenoxy derivatives-Histamine H3 receptor ligands, Bioorg. Med. Chem. Lett. 26 (16) (2016) 4140–4145, https://doi.org/10.1016/j.bmcl.2016.04.054.
[56] N. Levoin, et al., Determination of the binding mode and interacting amino-acids for dibasic H3 receptor antagonists, Bioorg. Med. Chem. 21 (2013) 4526–4529.
[57] R. Sheng, et al., Novel 1-phenyl-3-hydroxy-4-pyridinone derivatives as multifunctional agents for the therapy of Alzheimer's disease, ACS Chem. Neurosci. 7 (2015) 69–81.
[58] G. Wen, Q. Liu, H. Hu, D. Wang, S. Wu, Design, synthesis, biological evaluation, and molecular docking of novel flavones as H3 R inhibitors, Chem. Biol. Drug Des. 90 (4) (2017) 580–589, https://doi.org/10.1111/cbdd.2017.90.issue-410.1111/cbdd.12981.
[59] P. Panula, P.L. Chazot, M. Cowart, R. Gutzmer, R. Leurs, W.L.S. Liu, H. Stark, R. L. Thurmond, H.L. Haas, E.H. Ohlstein, International Union of Basic and Clinical Pharmacology, XCVIII. Histamine Receptors. *Pharmacol. Rev.* 67 (3) (2015) 601–655, https://doi.org/10.1124/pr.114.010249.
[60] K. Wingen, H. Stark, Scaffold variations in amine warhead of histamine H(3) receptor antagonists, Drug Discov. Today Technol. 10 (4) (2013) e483–e489, https://doi.org/10.1016/j.ddtec.2013.07.001.